Cell Biol Toxicol (2025) 41:61
https://doi.org/10.1007/s10565-025-10008-8

RESEARCH

CUL1-neddylation contributes to K29-linked ubiquitination on p27 for autophagic degradation in sorafenib-resistant liver cancer

Haitao Xu · Shaoyue Zheng · Qiuqi Zhang · Ying Xu · Hanbo Zhang · Tianming Hu · Xiaoling Zhang · Jiaoting E · Xuedong Li · Ruitao Wang · Hongyan Liu · Rui Xie

Received: 1 November 2024 / Accepted: 10 March 2025

Abstract Sorafenib has demonstrated great efficacy in liver cancer, however, its application as first-line treatment has been hampered due to the emerging drug resistance. This study is aimed to investigate the mechanism underlying acquired sorafenib resistance in liver cancer. Based on GSE109211 and TCGA datasets, bioinformatics analysis was conducted to find the potential genes implicated in the sorafenib resistance in liver cancer. mCherry-/eGFP-LC3B dual-fluorescent system was used to assess autophagic state. Wild and mutant types of HA-labeled ubiquitin (K27, K29, K33, K48, K63, K29R and K48R) were used to identify the type of polyubiquitin chains added to p27 by CUL1. Herein, we identified that F-box protein (SCF) ubiquitin ligase complexes (CUL1 and SKP2) and NEDD8 were highly expressed in sorafenib-resistant tissues using both the public data and clinical samples. NEDD8-mediated CUL1 neddylation enhanced SCF ubiquitin ligase complex to target p27 and subsequently linked K29-linked polyubiquitin chains to p27. Furthermore, NBR1 facilitated the degradation of ubiquitinated p27 protein by enhancing autophagy flux. Knocking down of CUL1 could prevent ubiquitination- and autophagy-mediated p27 protein degradation. The resistance to sorafenib was suppressed with CUL1 knockdown both *in vitro* and *in vivo*. In conclusion, our findings indicated that blocking neddylation or autophagy can restore drug sensitivity, thus providing a potential strategy for overcoming sorafenib resistance in the future.

Keywords Liver cancer · Sorafenib · Drug resistance · Autophagy · P27

Supplementary Information The online version contains supplementary material available at https://doi.org/10.1007/s10565-025-10008-8.

Haitao Xu, Shaoyue Zheng, and Qiuqi Zhang contributed equally to this work.

H. Xu
Department of Hepatobiliary and Pancreatic Surgery, Harbin Medical University Cancer Hospital, Harbin 150081, China

S. Zheng
Department of Endoscope, Harbin Medical University Cancer Hospital, Harbin 150081, China

Q. Zhang · Y. Xu · H. Zhang · T. Hu · X. Zhang · J. E · X. Li · R. Wang (✉) · H. Liu (✉) · R. Xie (✉)
Department of Internal Medicine, Harbin Medical University Cancer Hospital, Harbin 150081, China
e-mail: ruitao_wang@hrbmu.edu.cn

H. Liu
e-mail: 601999@hrbmu.edu.cn

R. Xie
e-mail: ruixie178@126.com; rxie@hrbmu.edu.cn

Published online: 20 March 2025

Introduction

Liver cancer is a highly malignant digestive system tumor with extremely poor prognosis. In 2023, approximately 41,210 new cases will be detected, leading to estimated 29,380 deaths (Siegel et al. 2023). Hepatocellular carcinoma (HCC) is the most common type of liver cancer, accounting for approximately more than 90% of all cases (Wu et al. 2012). HCC is generally caused by long-term liver damage resulting from chronic viral hepatitis infections, metabolic syndrome, non-alcoholic steatohepatitis, and exposure to toxins such as alcohol, aflatoxin, or pyrrolizidine alkaloids (McGlynn et al. 2021). Patients with HCC are commonly unable to receive early diagnosis and treatments due to their non-specific symptoms and aggressive behaviors. They generally result in poor outcomes with a 5-year survival rate as low as 10% (Sarveazad et al. 2019). Multiple therapeutic approaches, such as surgical resection, interventional ablation therapy, hepatic arterial chemoembolization, chemotherapy, and targeted therapy have been developed to increase patients' survival rates (Willatt et al. 2012). Unfortunately, the recurrence and metastasis rates after liver resection surgery were still high, and conventional chemotherapy was prone to drug resistance.

Sorafenib, a small molecule tyrosine kinase inhibitor, could inhibit tumor cell proliferation and angiogenesis by blocking the activities of Raf-1 and B-Raf serine-threonine kinases, as well as the receptor tyrosine kinase activities of vascular endothelial growth factor receptors (VEGFRs) and platelet-derived growth factor receptors (PDGFRs) (Wilhelm et al. 2008). Clinical trials have fully demonstrated that sorafenib could significantly increase the overall survival and time to progression in advanced HCC patients, with a nearly 3 months compared to placebo group (). Based on its remarkable efficacy, sorafenib was approved by the Food and Drug Administration in 2007, and has been considered as the standard of care for patients with advanced unresectable HCC. However, its wide clinical application often led to drug resistance, which greatly hindered the therapeutic efficacy. To date, the mechanism of sorafenib resistance remains unclear. Thus, it is imperative to investigate the mechanism to overcome the clinical dilemma in tumor treatment.

Herein, we investigated the molecular mechanism of sorafenib resistance in liver cancer cells. First, several hub genes were identified using the weighted gene co-expression network analysis (WGCNA), including CUL1, SKP2, NEDD8, as well as several autophagy receptors SQSTM1 and NBR1. These genes were upregulated in sorafenib-resistant tissues and may played important roles in the development of drug resistance. We then established the sorafenib-resistant cells and demonstrated the upregulated autophagy and downregulated p27 in these cells. In detail, the autophagy receptors such as SQSTM1 and NBR1 participated in the induction of ubiquitinated p27 protein entering lysosomal degradation. Knocking down of autophagy receptors could increase p27 expression and abrogate the high levels of autophagy. Moreover, blocking neddylation or autophagy could restore drug sensitivity, and the combination of both approaches resulted in the highest p27 levels and the strongest growth retardation in sorafenib-resistant cells.

To sum up, we demonstrated that blocking neddylation or autophagy could restore drug sensitivity of sorafenib-resistant cells, which held great promise for overcoming sorafenib resistance in the future.

Materials and methods

RNA sequencing and microarray data processing

The transcriptome data of RNA sequencing data and survival data were downloaded from the Gene Expression Omnibus database, TCGA, and cBioPortal database. The differential expression analysis between normal tissues and tumor tissues were obtained from GEPIA (Tang et al. 2017). The survival curves were calculated using the Kaplan–Meier plotter (Lanczky and Gyorffy 2021). The data matrix of gene expression in GSE109211 (Pinyol et al. 2019) was constructed by using "WGCNA" R package.

Cell culture and treatments

Liver cancer cell lines HepG2 and Huh7 were purchased from the Chinese Academy of Sciences (Shanghai, China), and cultured using the complete growth medium in a humidified incubator at 37 °C under an atmosphere of 5% CO_2. All human cell lines have been authenticated using STR profiling within the last three years, and all experiments were performed with mycoplasma-free cells. Sorafenib was purchased from Selleckchem (Shanghai, China). Bafilomycin A1 and MLN4924 was purchased from MedChemExpress (Shanghai, China). Cycloheximide was purchased from Sigma (Changsha, China). Wild and mutant types of HA-labeled ubiquitin (K27, K29, K33, K48, K63, K29R and K48R) were purchased from Addgene (Shanghai, China). Genepharma company (Shanghai, China) helped to constructed the siRNAs targeting to CUL1, NEDD8, SQSTM1 and MDM2 as well as expression vectors of CUL1, NBR1 and p27.

Western blot

Total protein extraction was performed using either a Total Protein Extraction Kit or RIPA lysis buffer for tissue and cell samples, respectively. The extracted proteins were separated by SDS-PAGE and transferred onto a nitrocellulose membrane, then blocked using 5% non-fat milk or BSA in TBST buffer, followed by incubation with primary antibodies (Table 1) overnight at 4 °C and an HRP-conjugated secondary antibody for 1–2 h at room temperature. Protein loading was normalized using β-actin or GAPDH as a loading control.

Table 1 List of antibodies used

Primary antibodies	MW (kDa)	Dilution	Source/ Catalog Number
CUL1	90/82	1:400	Thermo Fisher, 71–8700
NEDD8	9/90	1:1000	Abcam, ab81264
p21	21	1:500	Ptgcn, 10355–1-AP
p27	27	1:1000	Abcam, ab32034
LC3B	18/16	1:2000	Abcam, ab51520
Skp2	48	1:1000	CST, 2652
SQSTM1	62	1:1000	Ptgcn, 18420–1-AP
NBR1	37	1:500	Abcam, ab55474
OPTN	66	1:2000	Ptgcn, 10837–1-AP
NDP52	52	1:500	Ptgcn, 12229–1-AP
β-actin	42	1:2000	Ptgcn, 66009- 1-Ig

Real-time quantitative polymerase chain reaction (qPCR)

Total RNA was extract from cells or tissues using TRIzol reagent. The first strand cDNA was synthesized using RevertAid First Strand cDNA Synthesis Kit (Thermo, USA). qPCR was performed on reverse transcribed RNA samples to determine the expression level of the target gene (Table 2). The qPCR was performed using SYBR™ Green PCR Master Mix (Thermo, USA). The reaction was run for 40 cycles, including an initial denaturation step at 95℃ for 5 min, 94℃ for 20 s, 60℃ for 20 s, and 72℃ for 20 s. The gene expression level was determined using the $2^{-\Delta\Delta CT}$ method (Livak and Schmittgen 2001).

Cell counting kit 8 (CCK-8)

Cells were seeded in 96-well plates at a density of approximately 1×10^5 cells per well with 100 µl of culture medium for 48 h. Then, 10 µl of cell counting kit 8 solution (Beyotime, China) was added and the plate was incubated for 1 h. The absorbance was then measured at 450 nm using a microplate

Table 2 List of primers used

Primer	Primer Sequence (5′−3′)
CUL1-F	GGTTCGCCGTGAATGTGAC
CUL1-R	CCCCAATTCCACGTAAGACTGT
SKP2-F	ATGCCCCAATCTTGTCCATCT
SKP2-R	CACCGACTGAGTGATAGGTGT
SQSTM1-F	GACTACGACTTGTGTAGCGTC
SQSTM1-R	AGTGTCCGTGTTTCACCTTCC
NBR1-F	CAGTGCAGTCGTTTCCACTTG
NBR1-R	AGGTAGCTTGTGAACCAGTCT
p27-F	TAATTGGGGCTCCGGCTAACT
p27-R	TGCAGGTCGCTTCCTTATTCC
β-actin-F	ACCCTGAAGTACCCCATCGAG
β-actin-R	AGCACAGCCTGGATAGCAAC

reader. The cell proliferation rate was calculated using the formula: (OD of treated cells—OD of blank control) / (OD of control cells—OD of blank control) × 100%.

EdU cell proliferation assay

The EdU-555 cell proliferation assay was used to detect cell proliferation in this study. The Beyo-Click™ EdU Cell Proliferation Kit with Alexa Fluor 555 (Beyotime, China) was used to label cells with EdU. The labelled cells were subsequently detected using fluorescence microscopy.

The mCherry-/eGFP-LC3B dual-fluorescent autophagy detecting assay

The mCherry-eGFP-LC3B double-fluorescent autophagy indicator system was used to label by infection of the adenoviral mCherry-eGFP-LC3B plasmid cassette and track LC3 and autophagy changes. The decrease in GFP fluorescence indicates the degree of smoothness of autolysosome formation, while the constant expression of mCherry can be used to evaluate the progress of autophagy. The yellow spots obtained by merging red and green fluorescence images indicate autophagosomes, while red spots indicate autolysosomes. The strength of autophagy flow can be clearly observed by counting the number of spots of different colors.

Transwell assay

Cell invasion assay was performed using 24-well plates with 5 μm pore size and Matrigel basement membrane. Matrigel was diluted 1:8 with serum-free medium and coated onto the upper chamber of the transwell plate at 37℃ for 30 min. Then, the plate was placed into a 6-well plate with 1 mL of medium containing Fetal Bovine Serum in the bottom chamber. 5×10^4 cells in serum-free medium were seeded into the upper chamber. After incubation for a set period of time, the cells that invaded through the Matrigel and migrated to the lower chamber were fixed with 95% ethanol and stained with hematoxylin and eosin.

Colony-formation assay

Log-phase cells were digested and resuspended in the complete growth medium. The cells were then plated at a density of 500 cells per 3 cm dish with or without sorafenib. The cells were cultured for 2–3 weeks under 37 °C with 5% CO_2 and a humidified atmosphere, and the resulting colonies were counted and imaged. Colony-formation rate was calculated as the number of colonies divided by the number of cells seeded, multiplied by 100%.

Tumor xenograft analysis

Four-week-old male nude mice were purchased from Shanghai Experiment Animal Center (Shanghai, China). The mice were housed in pathogen-free barrier facility with a 12 h light/dark cycle and fed ad libitum with sterile chows and water. Animal tumor xenograft experiments involve injecting cells into the subcutaneous tissue of immunodeficient mice at a concentration of 1×10^6 cells per injection site, with a total volume of 200 μl. Each group consists of at least six randomly assigned mice. After approximately one week when the mice develop visible tumors, treatment with sorafenib (60 mg/kg) is initiated every 2 days via oral gavage for 2 weeks. Tumor size is measured every 3 days for 6 consecutive measurements, and the tumor volume is calculated using the formula $V = a \times b^2 \times 0.5^2$ (Sapi et al. 2015), where a and b are the longest and shortest diameters, respectively. The groups include A: HepG2-SR treated with saline, B: HepG2-SR treated with sorafenib, and C: HepG2-SR CUL1 knockdown cells treated with sorafenib.

Immunohistochemistry (IHC)

Briefly, 3 μm thick tissue sections were prepared and baked at 60–65 °C for 4 h. The sections were deparaffinized and rehydrated in a graded series of alcohols and water. Antigen retrieval was performed by high-pressure heating in citrate buffer (pH = 6) for 2 min. The sections were then incubated with blocking solution to prevent non-specific binding, followed by incubation with primary antibody (proliferating cell nuclear antigen, PCNA, 1:200; p27, 1:50; Proteintech, China) overnight at 4 °C. After washing with

PBS, the sections were incubated with biotinylated secondary antibody and streptavidin-HRP conjugate and developed with DAB substrate.

Statistical analysis

Data are presented as the mean ± SEM of three independent experiments. Unpaired Student t-test and one-way ANOVA were used for testing statistical differences among 2 or more than 2 treatment and control groups, respectively, via Prism GraphPad Prism software. $P < 0.05$ was considered statistically significant.

Result

Identification of hub genes associated with sorafenib resistance in HCC

To identify hub genes involved in the sorafenib resistance, we performed the WGCNA using the mRNA expression profiles of HCC patients in the GSE109211 dataset (Pinyol et al. 2019), which included a sorafenib treatment group ($n = 67$) and a placebo group ($n = 73$) (Fig. 1A and B). As a result, the brown module showed the strongest correlation with non-responders, with a Pearson correlation coefficient of 0.76 (Fig. 1C). Moreover, most genes in the brown module were upregulated in non-responders compared to responders (Fig. 1D). We then defined 35 hub genes with the module membership scores more than 0.85 and gene significance scores greater than 0.75 (Fig. 1E). To further determine the most important molecular players, we established a protein–protein interaction network using the 35 genes in STRING database, and identified 8 genes with the highest degree of connectivity in the network, including CUL1, SKP2, NBR1, NEDD8, PSMD4, PPP2R5C, VMP1, and PRMT1 (Fig. 1F). Intriguingly, CUL1 and SKP2 are key components of SCF complex (S: SKP2, C:CUL1 and F: F-box protein E3 ubiquitin ligases). CUL1 and SKP2 along with the genes NEDD8 for cullins neddylation formed a small network. In addition, NBR1, an autophagy receptor, was also included in the network.

Beyond that, we conducted enrichment analysis based on the differentially expressed genes between sorafenib non-responders ($n = 46$) and responders ($n = 21$). The results showed that upregulated genes in sorafenib non-responders were enriched in protein neddylation, ubiquitination, post-translational protein modification, and autophagy (Fig. 1G), which further verified the reasonability of the above network. Coordinating the above results, it was expected that these genes (CUL1, SKP2, NBR1, and NEDD8) may play many pivotal roles in sorafenib resistance.

To further explore the significance of these genes in HCC development and progression, we assessed their expression and prognostic implications in GSE144269 and TCGA cohorts. The results showed that CUL1, SKP2, and NEDD8 were not only highly expressed in cancerous than normal tissues but also elevated in sorafenib non-responders than responders in GSE109211 dataset (Fig. 1H and I). The high expression of these genes in tumor tissues were strongly associated with poor outcomes (Fig. 1J). There was a similar trend in TCGA cohort (Supplementary Fig. 1). Notably, all these genes were highly expressed in cancerous than normal tissues (Supplementary Fig. 1A) and the high expression of these genes in tumor tissues were strongly associated with poor outcomes in TCGA dataset (Supplementary Fig. 1B). It also should be noted that an E3 NEDD8 ligase MDM2 is not only increased in cancerous than normal tissues (Supplementary Fig. 1A) but also elevated in sorafenib non-responders than responders (Fig. 1I). Therefore, it might facilitate to the neddylation modification. Indeed, as indicated by western blot assay, the knockdown of MDM2 decreased the CUL1 neddylation, but had no effect on the total protein level of CUL1 and SKP2 (Supplementary Fig. 1C).

Expression levels of hub genes in HCC patients

To further investigate the expression of these genes, we collected the adjacent normal tissues and tumor tissues from 10 HCC patients who have been treated with or without sorafenib. We compared the gene expression in the normal tissues, primary tumor tissues (untreated with sorafenib)

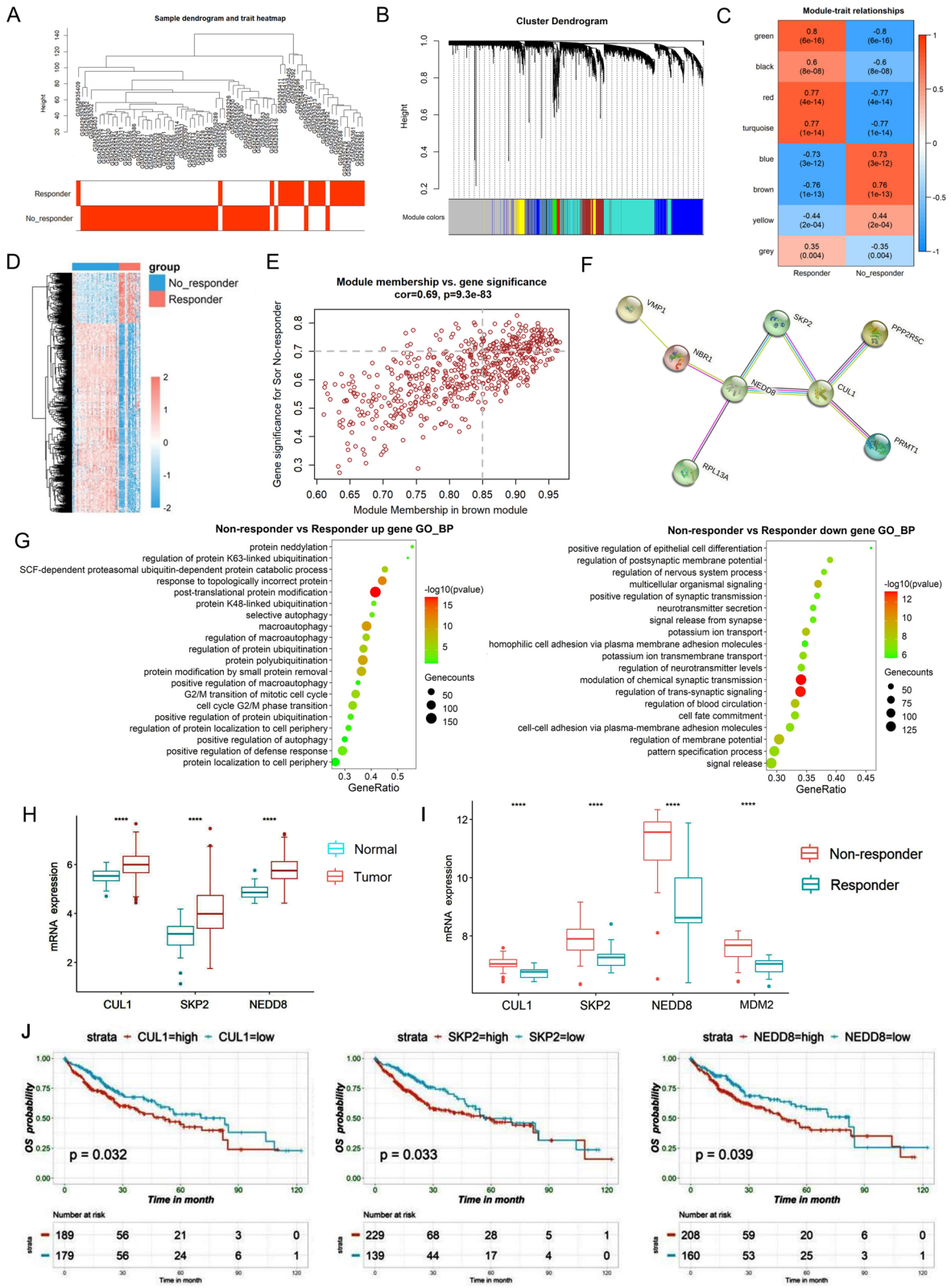
A
Sample dendrogram and trait heatmap
Height
Responder
No_responder
B
Cluster Dendrogram
Height
Module colors
C
Module-trait relationships
green
black
red
turquoise
blue
brown
yellow
grey
0.8 (6e-16)
-0.8 (6e-16)
0.6 (8e-08)
-0.6 (8e-08)
0.77 (4e-14)
-0.77 (4e-14)
0.77 (1e-14)
-0.77 (1e-14)
-0.73 (3e-12)
0.73 (3e-12)
-0.76 (1e-13)
0.76 (1e-13)
-0.44 (2e-04)
0.44 (2e-04)
0.35 (0.004)
-0.35 (0.004)
Responder
No_responder
D
group
No_responder
Responder
E
Module membership vs. gene significance
cor=0.69, p=9.3e-83
Gene significance for Sor No-responder
Module Membership in brown module
F
VMP1
NBR1
SKP2
PPP2R5C
NEDD8
CUL1
PRMT1
RPL13A
G
Non-responder vs Responder up gene GO_BP
protein neddylation
regulation of protein K63-linked ubiquitination
SCF-dependent proteasomal ubiquitin-dependent protein catabolic process
response to topologically incorrect protein
post-translational protein modification
protein K48-linked ubiquitination
selective autophagy
macroautophagy
regulation of macroautophagy
regulation of protein ubiquitination
protein polyubiquitination
protein modification by small protein removal
positive regulation of macroautophagy
G2/M transition of mitotic cell cycle
cell cycle G2/M phase transition
positive regulation of protein ubiquitination
regulation of protein localization to cell periphery
positive regulation of autophagy
positive regulation of defense response
protein localization to cell periphery
GeneRatio
-log10(pvalue)
Genecounts
Non-responder vs Responder down gene GO_BP
positive regulation of epithelial cell differentiation
regulation of postsynaptic membrane potential
regulation of nervous system process
multicellular organismal signaling
positive regulation of synaptic transmission
neurotransmitter secretion
signal release from synapse
potassium ion transport
homophilic cell adhesion via plasma membrane adhesion molecules
potassium ion transmembrane transport
regulation of neurotransmitter levels
modulation of chemical synaptic transmission
regulation of trans-synaptic signaling
regulation of blood circulation
cell fate commitment
cell-cell adhesion via plasma-membrane adhesion molecules
regulation of membrane potential
pattern specification process
signal release
GeneRatio
-log10(pvalue)
Genecounts
H
mRNA expression
Normal
Tumor
CUL1
SKP2
NEDD8
I
mRNA expression
Non-responder
Responder
CUL1
SKP2
NEDD8
MDM2
J
strata CUL1=high CUL1=low
OS probability
p = 0.032
Time in month
Number at risk
189 56 21 3 0
179 56 24 6 1
strata SKP2=high SKP2=low
OS probability
p = 0.033
Time in month
Number at risk
229 68 28 5 1
139 44 17 4 0
strata NEDD8=high NEDD8=low
OS probability
p = 0.039
Time in month
Number at risk
208 59 20 6 0
160 53 25 3 1

◂**Fig. 1** Identification of hub genes associated with sorafenib resistance in HCC. (**A**) The clustering dendrogram of sorafenib treatment responder and non-responder. (**B**) Color-represented clustering dendrogram of gene co-expression modules identified after using a merged dynamic tree cut. (**C**) Correlation between the sorafenib responsiveness and each module. (**D**) Heatmap of differentially expressed genes in the brown module. (**E**) Scatter diagram of genes in brown module. X-axis represents module membership, and Y-axis represents gene significance. (**F**) Identification of the most important proteins with the highest degree of connectivity within the protein–protein interaction network in STRING. (**G**) Enrichment analysis of differentially expressed genes between sorafenib non-responders and responders (left, upregulated; right, downregulated). (**H**) Box plots of CUL1, SKP2, and NEDD8 expression in GSE109211 cohort. (**I**) Expression of SCF E3 ubiquitin ligase complex components (CUL1, SKP2, and NEDD8) in sorafenib responders and non-responders in GSE109211 dataset. (**J**) Kaplan–Meier curves of HCC patients with high or low SKP2, CUL1, and NEDD8 expression in GSE109211 cohort

and tumor tissues (acquired drug resistance after sorafenib treatment). The PCR results showed no significant difference in expression of CUL1 and SKP2 between adjacent non-cancerous tissue and primary liver cancer tissue. However, CUL1 and SKP2 expression were higher in sorafenib-resistant tumors than in primary tumors (untreated with sorafenib) (Fig. 2A). As indicated by the western blot, CUL1 protein showed two bands with molecular weight 90KD and 85KD, respectively (Fig. 2B). The band of CUL1 protein with the molecular weight 90KD was significantly increased in the sorafenib-resistant tumor tissues compared to the primary tumor tissues, while no significant difference was observed in the band with molecular weight 85KD. The high molecular wight of CUL1 protein implies some protein modification. According to the evidence from the bioinformatics analysis, we tested the NEDD8-modified Cullin. NEDD8-Cullin and SKP2 were also significantly elevated in the sorafenib-resistant tumor tissues, compared to the primary tumor tissues. IHC assay showed that CUL1 was located in the cytoplasm in part of the cells, while, in other parts of cells, CUL1 was enriched in the cell nucleus (Fig. 2C). Based on the above results, it is conceived that post-translational modification such as neddylation in CUL1 was increased in sorafenib-resistant tumor.

CUL1 is involved in the sorafenib resistance in HCC

We previously established sorafenib-resistant cell lines by exposing liver cancer cells (HepG2 and Huh7 parental cells) to sorafenib stimulation for 6 months at concentrations lower than their respective half maximal inhibitory concentration (IC50) values (Zhai et al. 2014). The resultant cell lines were then continuously cultured in the presence of sorafenib to maintain their drug-resistant characteristics. The CCK-8 assay showed that IC50 values of HepG2 parental cells (HepG2-P) and HepG2 sorafenib-resistant cells (HepG2-SR) were 4.33 μM and 12.84 μM, respectively (Fig. 3A). IC50 values of Huh7 parental cells (Huh7-P) and Huh7 sorafenib-resistant cells (Huh7-SR) were 3.98 μM and 12.05 μM, respectively. The resistant cells exhibited apparent advantages in cell viability (Fig. 3A), proliferation (Fig. 3B and Supplementary Fig. 2A), colony formation capacity (Fig. 3C and Supplementary Fig. 2B), and invasion (Fig. 3D) under higher dosages of sorafenib treatment, further demonstrating the successful establishment of resistant cells. As shown in western blot assay, NEDD8-Cullin and SKP2 were also significantly elevated in the HepG2-SR and Huh7-SR cells than in HepG2-P and Huh7-P cells, respectively (Fig. 3E and Supplementary Fig. 2C). We knocked CUL1 down in the HepG2-SR and Huh7-SR cells (Fig. 3F). The knockdown of CUL1 remarkably enhanced the suppressive effect of sorafenib on the cell viability, proliferation, colony formation capacity and invasion (Fig. 3G-J and Supplementary Fig. 2D, E). These results collectively suggest that CUL1 is involved in the sorafenib resistance in HCC.

CUL1 neddylation mediates p27 ubiquitination in sorafenib-resistant liver cancer cells

The SCF complex is a subtype of Cullin-RING E3 ubiquitin ligase that includes CUL1 as its core

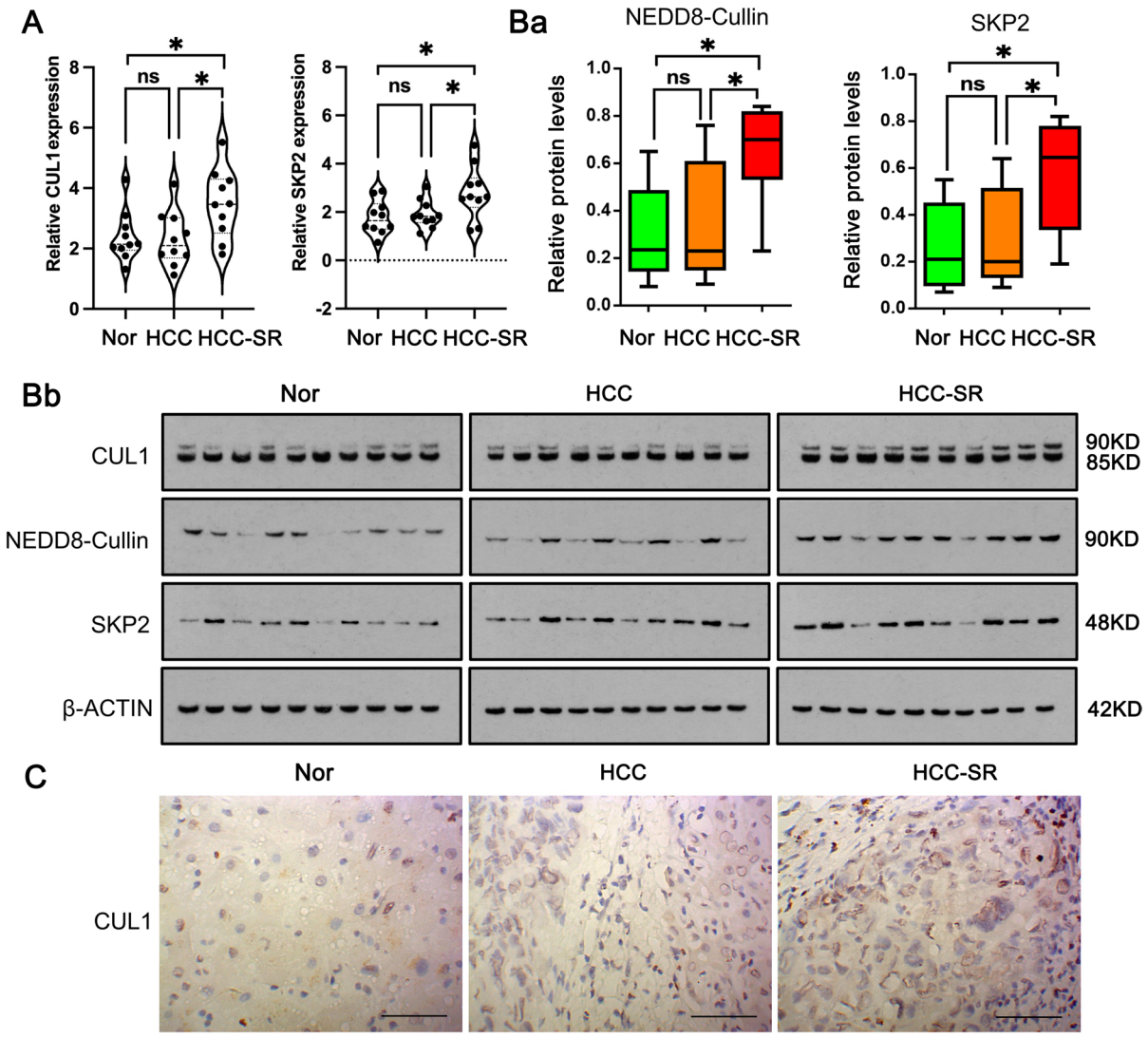

Fig. 2 Expression of SCF components in sorafenib-resistant liver tumors. (**A**) qPCR analysis of CUL1 and SKP2 in adjacent normal tissues, primary tumor tissues without sorafenib treatment, and primary tumor tissues resistant to sorafenib. (**B**) Western blot of the SCF E3 ubiquitin ligase complex components (CUL1 and SKP2) and NEDD8-Cullin in adjacent normal tissues, primary tumor tissues without sorafenib treatment, and primary tumor tissues resistant to sorafenib. (**C**) Representative IHC images of CUL1 in HCC patients.*$P<0.05$, **$P<0.01$ and ***$P<0.001$ ($n=10$)

Cullin protein. The E3 ligase facilitates the transfer of ubiquitin from E2 enzymes to target proteins, thus marking them for degradation by the proteasomes or lysosomes (Yang et al. 2021). The complete activation of ubiquitin ligases E3 ubiquitin ligases requires Cullin neddylation, a reversible modification by adding the ubiquitin-like protein NEDD8 to Cullins. Upon neddylation modification, ubiquitin ligases are activated to ubiquitinate specific substrates, such as various tumor suppressors (Enchev et al. 2015). p27 is a cyclin-dependent inhibitor that hindered the assembly and activity

of cyclin-dependent kinases and cyclin complexes, thus inducing cell cycle arrest and inhibiting cell proliferation, finally causing cell apoptosis (Parazzi et al. 2015). However, p27 is usually degraded by SCF complex in cancer, leading to the uncontrolled proliferation of cancer.

Given the increased expression of SCF component proteins in sorafenib-resistant cells, it was hypothesized a decrease in p27 as a result of CUL1 neddylation-mediated ubiquitination and degeneration. To test this hypothesis, the resistant cells were treated with a neddylation inhibitor, MLN4924 (Zheng et al. 2021). Western blot results showed a significant decrease in NEDD8 and CUL1 expression, while MLN4924 treatment had little effect on SKP2 expression (Fig. 4A and Supplementary Fig. 3A). Notably, p27 expression was restored in resistant cells in a dose-dependent manner (Fig. 4A and Supplementary Fig. 3A). Moreover, the co-immunoprecipitation results showed the reduced amounts of p27-immunoprecipitated CUL1 and ubiquitin in the presence of MLN4924 (1 μM, Fig. 4B) or under the conditions of silencing NEDD8 or CUL1 expression (Fig. 4C), suggesting that the restoration of p27 expression was attributed to a break of CUL1-mediated ubiquitination on p27. Instead, overexpressing CUL1 significantly increased p27 ubiquitination and decreased its protein expression in sorafenib-resistant cells, which could be reversed by MLN4924(1 μM, Fig. 4C). As a result, p27, which was otherwise quickly degraded in resistant cells, was largely stabilized after MLN4924 treatment (1 μM, Fig. 4D and Supplementary Fig. 3B) or when knocking down of NEDD8 or CUL1 (Fig. 4E and Supplementary Fig. 3C), respectively.

Hyperactive autophagy in sorafenib-resistant liver cancer cells

As shown in the results in Fig. 1F, CUL1, SKP2 and NEDD8 were linked to autophagy receptor, NBR1. Apart from it, several genes closely related to autophagy, such as *SQSTM1*(also known as *p62*), *OPTN* and *NDP52* were also increased in tumor tissues compared to normal tissues in GSE144269 and TCGA datasets (Fig. 5A). Moreover, NBR1, SQSTM1, OPTN and NDP52 mRNA were increased in the sorafenib-resistant tumor tissues compared to the primary tumor tissues in GSE144269 datasets. The increased NBR1 and SQSTM1 mRNA were further identified in the sorafenib-resistant tissues compared to the primary tissues (Fig. 5B). However, except the increased protein levels of OPTN, the protein levels of NBR1 and SQSTM1 were decreased in the sorafenib-resistant cells (Fig. 5E and Supplementary Fig. 4A) and tissues (Fig. 5C and D). Therefore, we conjectured that the increased NBR1 and SQSTM1 mRNA contributes to their protein levels and the formation of autophagosomes in early autophagy, but the degradation of autophagosomes in lysosomes in later autophagy leads to the final reduction of NBR1 and SQSTM1 proteins. To validate the conjecture, we used the mCherry-/eGFP-LC3B dual-fluorescent autophagy indicator system to assess autophagic state. In detail, yellow spots represent autophagosomes, and the red spots represent autolysosomes (the fusion of autophagosomes with lysosomes) (Hua et al. 2015). The microscope imaging showed that sorafenib-resistant cells had hyperactive autophagy compared to the parental cells, as evidenced by the enhanced yellow and red spots (Fig. 5F). Autophagy inhibitor Bafilomycin A1 (BafA1) blocks the formation of autophagic lysosomes and prevents the degradation of autophagy receptor proteins (Mauvezin and Neufeld 2015). The application of BafA1 induced the formation of autophagosomes but prevented their subsequent fusion with lysosomes, as indicated by the increased yellow spots and decreased red spots. Rapamycin (RAP) is an autophagy activator (Huang et al. 2015; Lin et al. 2018). Treatment with RAP increased the yellow and red spots in sorafenib-resistant cells, suggesting that it further enhances the formation of autophagosomes and autolysosomes. The microtubule-associated proteins light chain 3B (LC3B) is important in the formation of autophagosomes. The western blot results showed that LC3B-II was upregulated in both sorafenib-resistant cells than

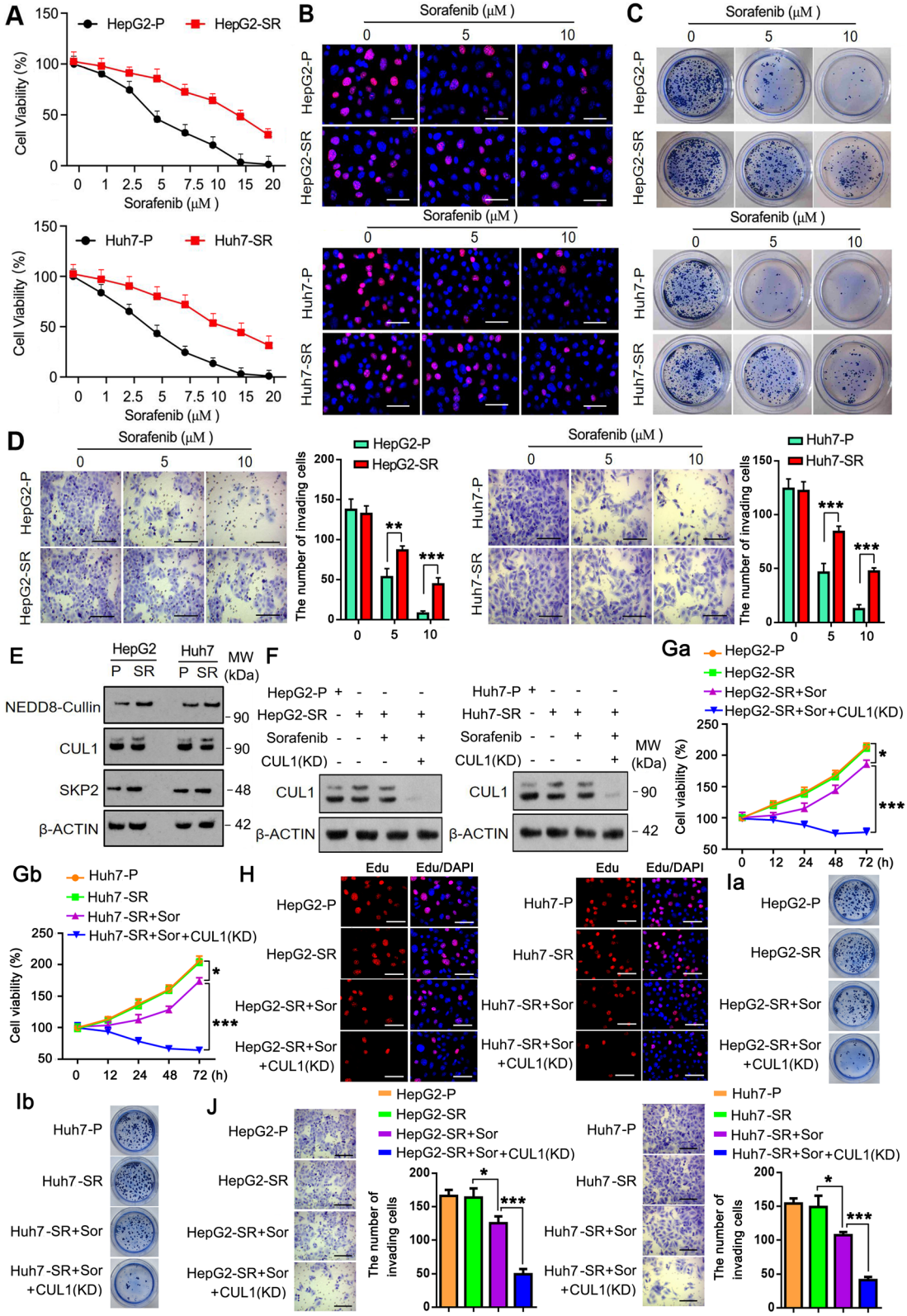
A
HepG2-P
HepG2-SR
Cell Viability (%)
Sorafenib (μM)
Huh7-P
Huh7-SR
B
Sorafenib (μM)
HepG2-P
HepG2-SR
Huh7-P
Huh7-SR
C
Sorafenib (μM)
HepG2-P
HepG2-SR
Huh7-P
Huh7-SR
D
Sorafenib (μM)
HepG2-P
HepG2-SR
The number of invading cells
Huh7-P
Huh7-SR
E
HepG2
Huh7
P SR P SR
MW (kDa)
NEDD8-Cullin
CUL1
SKP2
β-ACTIN
F
HepG2-P
HepG2-SR
Sorafenib
CUL1(KD)
Huh7-P
Huh7-SR
CUL1
β-ACTIN
Ga
HepG2-P
HepG2-SR
HepG2-SR+Sor
HepG2-SR+Sor+CUL1(KD)
Cell viability (%)
Gb
Huh7-P
Huh7-SR
Huh7-SR+Sor
Huh7-SR+Sor+CUL1(KD)
H
Edu
Edu/DAPI
HepG2-P
HepG2-SR
HepG2-SR+Sor
HepG2-SR+Sor +CUL1(KD)
Huh7-P
Huh7-SR
Huh7-SR+Sor
Huh7-SR+Sor +CUL1(KD)
Ia
Ib
J
The number of invading cells

◂**Fig. 3** CUL1 is involved in the sorafenib resistance in HCC. (**A**) CCK-8 assay of parental cells (HepG2-P and Huh7-P) and sorafenib-resistant cells (HepG2-SR and Huh7-SR) in the presence of gradient sorafenib treatment. (**B**) EdU assay, (**C**) colony formation assay, and transwell assay (**D**) of HepG2-P, Huh7-P, HepG2-SR and Huh7-SR cells under 0, 5, and 10 μM sorafenib treatment. (**E**) Western blot of SCF components (CUL1 and SKP2), and NEDD8-Cullin in HepG2 and Huh7 parental cells and their corresponding sorafenib-resistant cells. (**F**) Western blot test of CUL1 after sorafenib treatment and CUL1 knockdown. (**G**) CCK-8 assay, (**H**) EdU assay, (**I**) colony formation assay, and transwell assay (**J**) of HepG2-P, Huh7-P, HepG2-SR and Huh7-SR cells after sorafenib treatment and CUL1 knockdown. $^{*}P<0.05$, $^{**}P<0.01$ and $^{***}P<0.001$ ($n=3$). Sor:sorafenib; KD: knockdown

in their parental cells (Fig. 5G and Supplementary Fig. 4B). RAP treatment increased both LC3B-I and LC3B-II in sorafenib-resistant cells, which was similar to the effect by BafA1. However, RAP treatment further decreased NBR1 and SQSTM1 proteins in the sorafenib-resistant cells, while BafA1 increased the protein levels of NBR1 and SQSTM1. These results suggested that NBR1 and SQSTM1 are indeed degradated in the lysosomes in the sorafenib-resistant cells due to the enhanced autophagy.

p27 was largely decreased in the resistant cells. After the intervention of BafA1, the protein expression of p27 was upregulated (Fig. 5G and Supplementary Fig. 4B). Instead, RAP further decreased p27 in the resistant cells. These results suggested that p27 protein level is related to the enhanced autophagy in the sorafenib-resistant cells. Notely, the qPCR data showed no between-group variance in p27 expression, while CUL1 and SKP2 mRNA were upregulated in all resistant cell groups (Supplementary Fig. 5), indicating that the expression changes of p27 did not occur at the transcription level.

Cul1 induces K29-linked ubiquitination on p27, resulting in the autophagic degradation in sorafenib-resistant liver cancer cells

Autophagy is a lysosome-degradation program where the double-membrane autophagosomes are formed in the cytoplasm to sequester cellular components (Chen et al. 2019a). Considering the hyperactive autophagic state of sorafenib-resistant cells (Figs. 3E-H), we postulated that CUL1 neddylation-mediated ubiquitination leads to the autophagy-mediated lysosomal degradation of p27 in the resistant cells, though ubiquitination usually induces the degradation of p27 in proteasomes. Previous reports have shown that MLN4924 (1 μM) induces autophagy in liver cancer cells (Luo et al. 2012). Our western blot assay showed a higher level of LC3B in MLN4924-treated sorafenib-resistant cells than untreated cells (Fig. 6A). Consistent with this, microscope imaging data also indicated an increased formation of autophagosomes in the presence of MLN4924 (1 μM, Fig. 6B). However, little or no difference was observed in terms of the amount of autophagic lysosomes, as evidenced by an increase in yellow but not red spots in MLN4924-treated cells (Fig. 6B). These results together revealed that MLN4924, a NEDD8-activating enzyme inhibitor, can promote autophagosome formation, but fail to promote autophagic flux effectively.

To distinguish between autophagy- and ubiquitination-mediated p27 protein degradation, we pre-treated sorafenib-resistant cells with BafA1 or proteasome inhibitor MG132. The former blocks the formation of autophagic lysosomes (Yang et al. 2021), while the latter inhibits ubiquitin–proteasome system-mediated protein degradation (Lee and Goldberg 1998). Next, the cells were explored to the protein synthesis inhibitor cycloheximide. Finally, p27 expression at different time points were examined using western blot assay. It was discovered that p27 protein was quickly degraded in untreated cells (Fig. 6C and Supplementary Fig. 6A). However, BafA1 and MG132 were able to extend the stability of p27 protein, with BafA1 exhibiting a stronger stabilizing effect than MG132 (Fig. 6C and Supplementary Fig. 6A). Thus, the autophagy, which is activated after gaining drug-resistance, plays more important role in p27 protein degradation.

The expression of autophagy receptors (SQSTM1, NBR1, and OPTN) was different in the

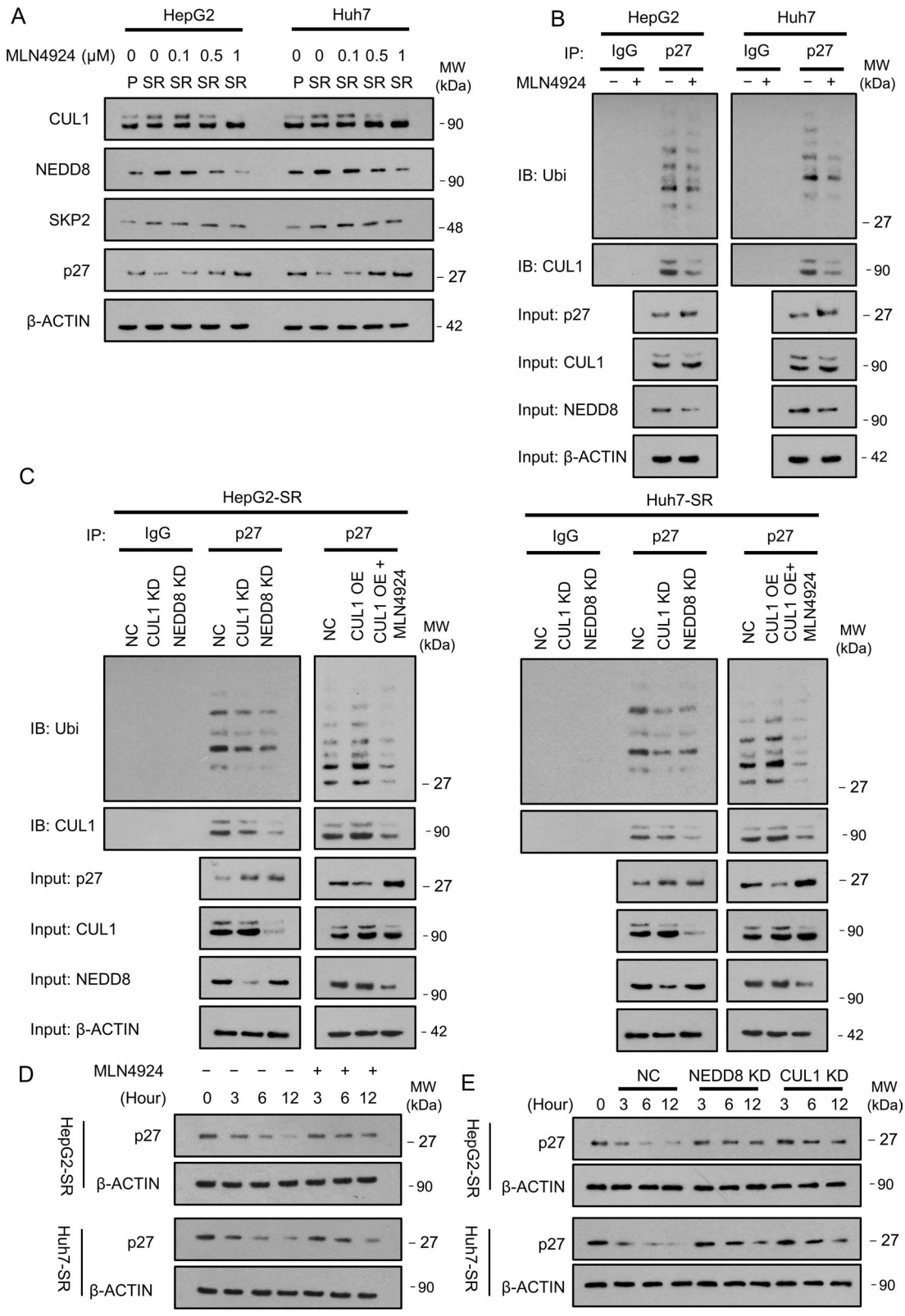
A
HepG2
Huh7
MLN4924 (μM) 0 0 0.1 0.5 1 0 0 0.1 0.5 1
P SR SR SR SR P SR SR SR SR
MW (kDa)
CUL1
NEDD8
SKP2
p27
β-ACTIN
90
90
48
27
42
B
HepG2
Huh7
IP: IgG p27 IgG p27
MLN4924 − + − + − + − +
MW (kDa)
IB: Ubi
IB: CUL1
Input: p27
Input: CUL1
Input: NEDD8
Input: β-ACTIN
27
90
27
90
90
42
C
HepG2-SR
Huh7-SR
IP: IgG p27 p27
NC CUL1 KD NEDD8 KD NC CUL1 KD NEDD8 KD NC CUL1 OE CUL1 OE + MLN4924
MW (kDa)
IB: Ubi
IB: CUL1
Input: p27
Input: CUL1
Input: NEDD8
Input: β-ACTIN
27
90
27
90
90
42
D
MLN4924 − − − − + + +
(Hour) 0 3 6 12 3 6 12
MW (kDa)
HepG2-SR
Huh7-SR
p27
β-ACTIN
27
90
E
NC NEDD8 KD CUL1 KD
(Hour) 0 3 6 12 3 6 12 3 6 12
MW (kDa)
HepG2-SR
Huh7-SR
p27
β-ACTIN
27
90

◂**Fig. 4** CUL1 neddylation mediates p27 ubiquitination in sorafenib-resistant liver cancer cells. (**A**) Western blot of SCF components (CUL1 and SKP2), NEDD8-Cullin, and p27 in sorafenib-resistant cells and their corresponding parental cells in the absence or presence of gradient neddylation inhibitor, MLN4924. (**B, C**) Co-immunoprecipitation analysis demonstrated the changes in the amounts of p27-immunoprecipitated CUL1 and ubiquitin under the conditions of MLN4924 treatment (1 μM) (**B**), NEDD8 or CUL1 silencing or overexpressing (**C**). (**D, E**) Western blot showed increased p27 protein stability in sorafenib-resistant cells under the conditions of MLN4924 treatment (1 μM) (**D**), NEDD8 or CUL1 silencing (**E**)

drug-resistant tissues and cells compared to the primary tissues and cells (Fig. 5E). Therefore, they might be implicated the autophagic degradation of p27. To validate it, we knocked down each individual receptor in the resistant cells. The results showed that p27 expression was largely induced after NBR1 knockdown, and to a less great extent upon SQSTM1 knockdown (Fig. 6D and Supplementary Fig. 6B). Silencing of OPTN showed little influence on p27 expression (Fig. 6D and Supplementary Fig. 6B). Consistently, SQSTM1 knockdown greatly abrogated high basal level of autophagy in sorafenib-resistant cells by inhibiting autophagic lysosome formation (Fig. 6E). In detail, there was increased yellow spots with decreased red spots in SQSTM1 knockdown cells versus the untreated cells (Fig. 6E). Interestingly, overexpression of NBR1 rescued the reduced autophagic flow in SQSTM1 knockdown cells, as evidenced by more prominent red spots in dual-fluorescent autophagy indicator system (Fig. 6E) and the reduced p27 protein levels in western blot assay (Fig. 6F and Supplementary Fig. 6C). Moreover, ectopic NBR1 expression alone was sufficient to induce autophagic flow according to the increased red to yellow spots ratio (Fig. 6E) and p27 protein expression (Fig. 6F and Supplementary Fig. 6C). This effect could be abrogated in the presence of BafA1, the inhibitor of autophagic lysosomes formation (Fig. 6F and Supplementary Fig. 6C).

Ubiquitin is a protein of 76 amino acids with 7 lysine residues (K6, K11, K27, K29, K33, K48, and K63), all of which can be ubiquitinated to form ubiquitin polyubiquitin chains. Different polyubiquitin chains determine the fate of substrate proteins, such as whether the protein is degraded by autophagic lysosomes or ubiquitin–proteasome system. To determine the types of polyubiquitin chains on p27, we transfected HepG2-SR cells with wild and mutant types of HA-labeled ubiquitin. For the mutant ubiquitins, polyubiquitin chains are linked only at one of the lysine residues (K27, K29, K33, K48 and K63) as the other lysine residues are mutant to arginine. As indicated by co-immunoprecipitation, the polyubiquitin chains on p27 can be linked by K27, K29, K33, K48 and K63 (Fig. 6G). However, knockdown of CUL1 decreased the polyubiquitin chains linked by K29 on p27 (Fig. 6G). We also transfected HepG2-SR cells with mutant types of HA-labeled ubiquitin, K29R and K48R (Fig. 6H). For two mutant ubiquitin, the polyubiquitin chains can be linked by any lysine residues, except from the K29 and K48 respectively. Overexpression of His-labeled CUL1 induced the addition of the K29-linked polyubiquitin chains to p27, but had minor effect once K29 was mutant to K29R. Overexpression of His-labeled CUL1 also induced the addition of the K48-linked polyubiquitin chains to p27, which is not influenced by the mutation of K48 to R48. These results collectively suggest that CUL1 primarily induces K29-linked ubiquitination on p27.

This study conducted Co-IP to determine whether K29-linked ubiquitination on p27 contributes the binding of p27 to NBR1 and SQSTM1. HA-labeled ubiquitin (K29) and Flag-label p27 vectors were transfected to HepG2-SR cells. Knockdown of CUL1 decreased the polyubiquitin chains linked by K29 on p27. Importantly, the enrichment of NBR1 and SQSTM1 binding to p27 was also decreased with CUL1 knockdown (Supplementary Fig. 6D).

Blocking neddylation and CUL1-NBR1 restores drug sensitivity in sorafenib-resistant cells

Since CUL1 neddylation and subsequent CUL1-NBR1-mediated autophagic degradation significantly influences p27 protein level, we investigated that whether restoring p27 expression by suppression of neddylation and knockdown of CUL1 affects the development of sorafenib resistance in

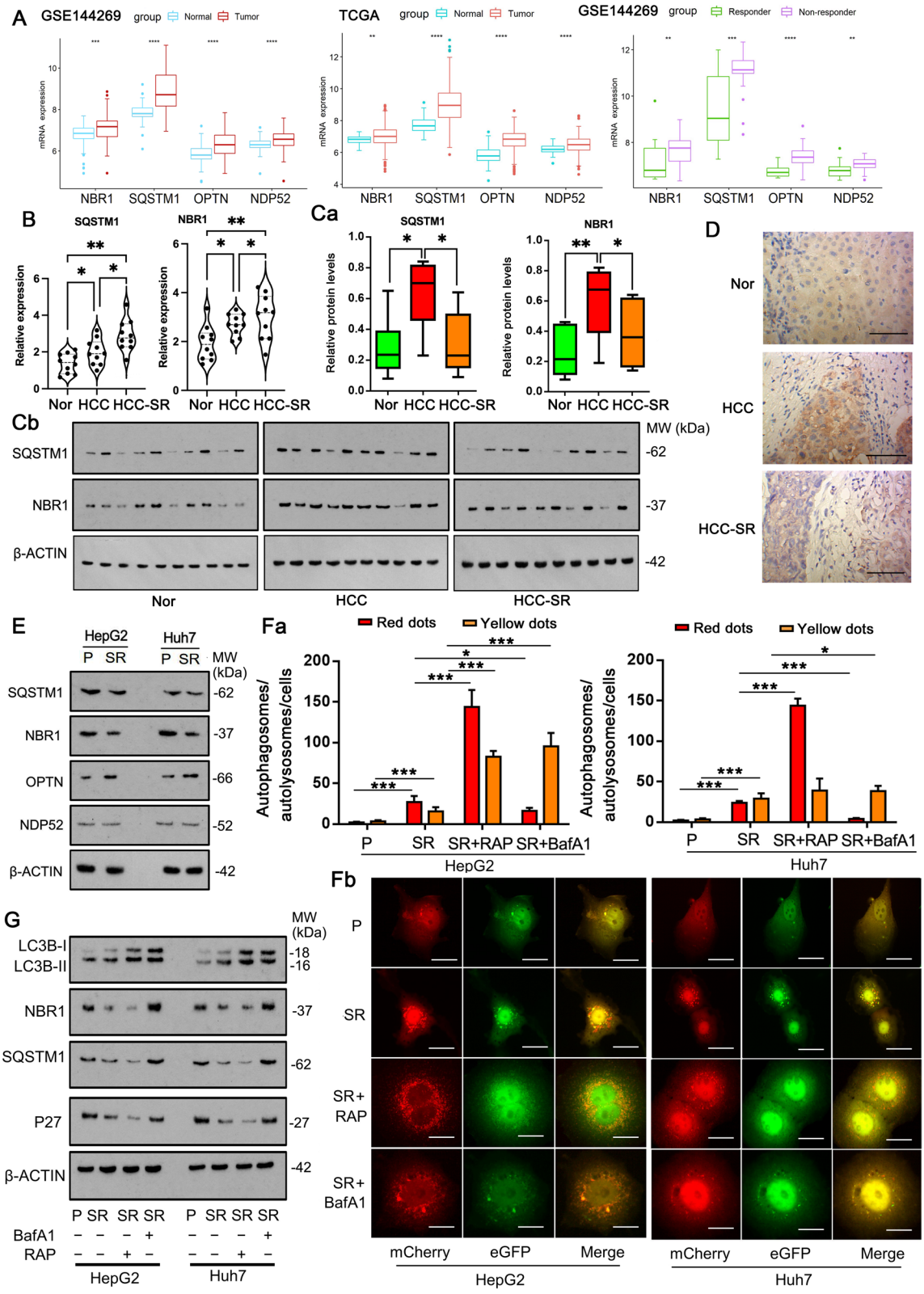
A
GSE144269 group Normal Tumor
TCGA group Normal Tumor
GSE144269 group Responder Non-responder
mRNA expression
NBR1 SQSTM1 OPTN NDP52
B
SQSTM1
NBR1
Relative expression
Nor HCC HCC-SR
Ca
SQSTM1
NBR1
Relative protein levels
Nor HCC HCC-SR
Cb
MW (kDa)
SQSTM1
NBR1
β-ACTIN
-62
-37
-42
Nor
HCC
HCC-SR
D
Nor
HCC
HCC-SR
E
HepG2
Huh7
P SR
MW (kDa)
SQSTM1
NBR1
OPTN
NDP52
β-ACTIN
-62
-37
-66
-52
-42
Fa
Red dots Yellow dots
Autophagosomes/ autolysosomes/cells
P SR SR+RAP SR+BafA1
HepG2
Huh7
Fb
P
SR
SR+ RAP
SR+ BafA1
mCherry eGFP Merge
HepG2
Huh7
G
MW (kDa)
LC3B-I
LC3B-II
NBR1
SQSTM1
P27
β-ACTIN
-18
-16
-37
-62
-27
-42
P SR SR SR P SR SR SR
BafA1 − − − + − − − +
RAP − − + − − − + −
HepG2
Huh7

◂**Fig. 5** Hyperactive autophagy in sorafenib-resistant liver cancer cells. Box plots of autophagy receptors in normal tissues, primary tumor tissues, sorafenib responders and non-responders in GSE109211 and TCGA cohorts. (**B**) qPCR analysis of SQSTM1 and NBR1 in adjacent normal tissues, primary tumor tissues without sorafenib treatment, and primary tumor tissues resistant to sorafenib. (**C**) Western blot of the SQSTM1 and NBR1 in adjacent normal tissues, primary tumor tissues without sorafenib treatment, and primary tumor tissues resistant to sorafenib. (**D**) Representative IHC images of NBR1 in HCC patients. (**E**) Western blot of the autophagy receptors in HepG2-P, Huh7-P, HepG2-SR and Huh7-SR cells. (**F**) Representative immunofluorescence images captured in the mCherry-/eGFP-LC3B dual-fluorescent autophagy indicator system. Yellow spots represent autophagosomes, and the red spots represent autolysosomes. (**G**) Western blot of LC3B (autophagic activity marker), autophagy receptors and the cyclin-dependent inhibitor p27 in parental and resistant cell lines with or without BafA1 and Rapamycin treatments. Rapamycin (RAP) was used as an autophagy activator. $*P<0.05$, $**P<0.01$ and $***P<0.001$ ($n=3$)

liver cancer cells. We observed that the sensitivity of the sorafenib was regained by either adding neddylation inhibitor MLN4924 (1 μM) or knocking down CUL1 in sorafenib-resistant cells in terms of cellular proliferation (Fig. 7A and Supplementary Fig. 7A), colony-formation (Fig. 7B and Supplementary Fig. 7B) and invasion (Fig. 7C). These interventions were also able to prevent p27 degradation in the resistant cells (Fig. 7D and Supplementary Fig. 7C). Importantly, the combination of MLN4924 (1 μM) and CUL1 knockdown resulted in the strongest suppression of growth, colony-formation and invasion, as well as the highest p27 protein levels in the presence of sorafenib. However, the regained drug sensitivity of sorafenib-resistant cells achieved by CUL1 knockdown was reversible when overexpressing NBR1 and knocking down p27, as indicated by the enhanced cell growth (Fig. 7E and Supplementary Fig. 7D), colony-formation (Fig. 7F and Supplementary Fig. 7E) and invasion (Fig. 7G), and decreased p27 protein levels (Fig. 7H). CUL1 knockdown reduced the immunofluorescence of p27 merged with the immunofluorescence of lysosomes, suggesting that CUL1 knockdown suppressed the transport of p27 to lysosomes (Fig. 7I). However, overexpressing NBR1 attenuated the effect by CUL1 knockdown.

Finally, we examined the therapeutic efficacy in vivo using the xenografted mouse model. As expected, subcutaneous injection of sorafenib-resistant HepG2 cells resulted in apparent tumor growth in the transplanted mice (Fig. 7J and K). Every other day-gavage delivery of sorafenib ameliorates the tumor burden brought by the drug-resistant cells. Knockdown of CUL1 largely sensitized cells' response to sorafenib treatment, leading to a greatly reduced xenograft tumor size. Moreover, large tumors in the drug-resistant HepG2 transplanted mice exhibited strong nuclear immunostaining of proliferation marker proliferating cell nuclear antigen (ki67) but weak p27, regardless of sorafenib administration. In contrast, CUL1 knockdown tumors showed little ki67 staining but more strikingly increased p27 staining (Fig. 7L).

Discussion

Since the approvement by Food and Drug Administration for the treatment of HCC in 2007, sorafenib has been considered the standard of care for patients with advanced unresectable HCC (). Till recently, a couple of other drugs such as brivanib (the dual inhibitor of VEGFR and fibroblasts growth factor receptors) (Johnson et al. 2013), sunitinib (the multi-targeted receptor tyrosine kinase inhibitor) (Cheng et al. 2013), linifanib (the inhibitor of VEGFR and PDGFR) (Cainap et al. 2015), and lenvatinib (the inhibitor of VEGFR1-3, fibroblasts growth factor receptors 1–4, PDGFRα, RET, and KIT) (Kudo et al. 2018), have been compared with sorafenib as first-line treatment for HCC patients. Unfortunately, none of these drugs exhibited superiority to sorafenib in the phase 3 trials, and sorafenib remains a cornerstone treatment in HCC. However, in the clinical trials which were pivotal in the approval of sorafenib (), about 30% of patients shown different sensitivity to the treatment, suggesting the inherent or acquired drug resistance in HCC patients (Chen et al. 2019b).

Recent studies reported the role of regulated cell death in the initiation and development of sorafenib resistance (Tang et al. 2020). Regulated cell death

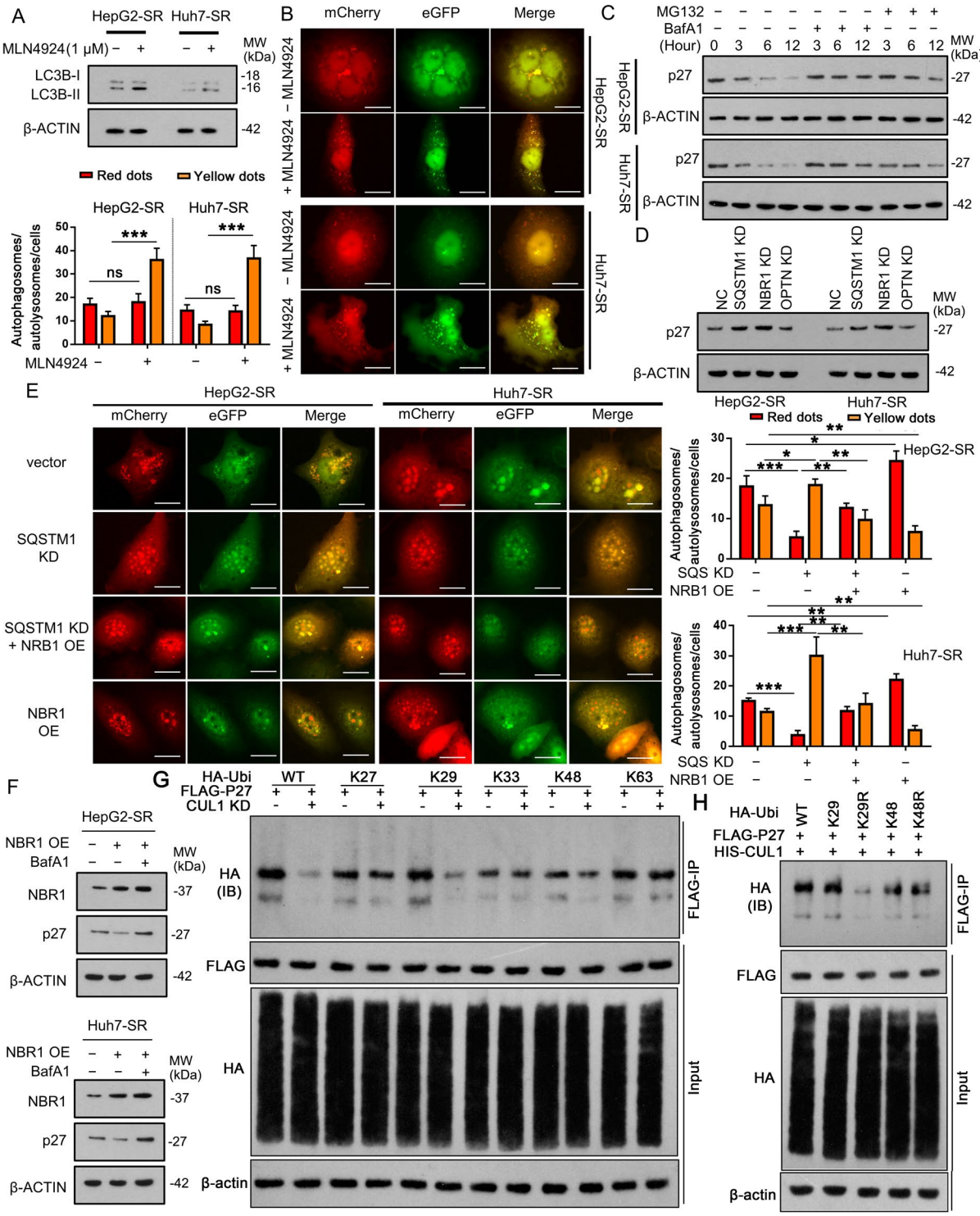
A
HepG2-SR Huh7-SR
MLN4924 (1 μM) − + − +
MW (kDa)
LC3B-I
LC3B-II
-18
-16
β-ACTIN
-42
Red dots
Yellow dots
HepG2-SR
Huh7-SR
Autophagosomes/ autolysosomes/cells
***
ns
MLN4924
B
mCherry
eGFP
Merge
− MLN4924
+ MLN4924
HepG2-SR
Huh7-SR
C
MG132
BafA1
(Hour) 0 3 6 12 3 6 12 3 6 12
MW (kDa)
p27
-27
β-ACTIN
-42
D
NC
SQSTM1 KD
NBR1 KD
OPTN KD
E
vector
SQSTM1 KD
SQSTM1 KD + NRB1 OE
NBR1 OE
SQS KD
NRB1 OE
F
HepG2-SR
NBR1 OE
BafA1
NBR1
-37
p27
-27
β-ACTIN
-42
Huh7-SR
G
HA-Ubi
FLAG-P27
CUL1 KD
WT
K27
K29
K33
K48
K63
HA (IB)
FLAG
HA
β-actin
FLAG-IP
Input
H
HA-Ubi
FLAG-P27
HIS-CUL1
WT
K29
K29R
K48
K48R

◂**Fig. 6** CUL1 induces K29-linked ubiquitination on p27, resulting in the autophagic degradation in sorafenib-resistant liver cancer cells (**A**) Western blot of autophagic activity marker LC3B in sorafenib-resistant liver cancer cells upon MLN4924 treatment (1 μM). (**B**) Immunofluorescence images demonstrated increased formation of autophagosomes but not the amount of autophagic lysosomes in MLN4924-treated cells (1 μM). (**C**) Western blot of p27 protein in sorafenib-resistant cells in the presence of BafA1 or MG132. (**D**) Western blot of p27 protein in sorafenib-resistant cells when silencing the autophagy receptors. (**E**) Immunofluorescence images showed abrogated basal autophagy by knocking down SQSTM1 in sorafenib-resistant cells, which was reversible upon over-expressing NRB1. (**F**) Western blot of p27 protein in SQSTM1 knockdown cells when over-expressing NBR1 with or without BafA1 treatment. (**G**) HepG2-SR cells were transfected with wild and mutant types of HA-labeled ubiquitin. For the mutant ubiquitins, polyubiquitin chains are linked only at one of the lysine residues (K27, K29, K33, K48 and K63) as the other lysine residues are mutant to arginine. In addition, cells were transfected with FLAG-labeled p27 with or without CUL1 knockdown. Co-immunoprecipitation was conducted to determine the types of polyubiquitin chains on p27. (**H**) HepG2-SR cells were transfected with mutant types of HA-labeled ubiquitin, K27, K29, K29R and K48R. For the mutant K27 and K29 ubiquitins, polyubiquitin chains are linked only at K27 and K29 respectively, as the other lysine residues are mutant to arginine. For mutant K29R and K48R ubiquitin, the polyubiquitin chains can be linked by any lysine residues, except from the K29 and K48 respectively. In addition, cells were transfected with FLAG-labeled p27 and HIS-labeled CUL1. Co-immunoprecipitation was conducted to determine the types of polyubiquitin chains on p27. $*P<0.05$, $**P<0.01$ and $***P<0.001$ ($n=3$)

includes apoptosis, ferroptosis, proptosis, and autophagic cell death, among which, autophagy is a crucial process that facilitates the breakdown and recycling of damaged organelles, misfolded proteins, and other cellular components by lysosomes in eukaryotic cells (Das et al. 2012). The impact of autophagy on cancer cells is complex, as it can both suppress and promote cancer development. In normal cells, basic autophagy serves as a cancer suppressor by maintaining genomic stability, whereas activated autophagy can support the survival of cancer cells under stress (Liu et al. 2016; White and DiPaola 2009; Shintani and Klionsky 2004). In contrast, ubiquitin-mediated protein degradation is a process that targets specific proteins for degradation by the proteasome, a large protein complex that breaks down proteins into smaller peptides (Ciechanover and Schwartz 1998). Ubiquitin is a small protein that is covalently attached to target proteins, marking them for degradation. Autophagy and ubiquitin–proteasome-mediated protein degradation are two critical processes that play essential roles in maintaining cellular homeostasis. Both autophagy and ubiquitin–proteasome-mediated protein degradation are tightly regulated and interconnected, with evidence suggesting that they can work together to regulate protein degradation (Kocaturk and Gozuacik 2018). We postulate that the enhanced basal autophagy in sorafenib-resistant liver cancer cells could be resulted from the drug-induced cell stresses. Indeed, sorafenib enhanced the temozolomide sensitivity of human glioma cells by inducing oxidative stress-mediated autophagy (Wei et al. 2021). Future work specifying stress type such as genotoxic stress, endoplasmic reticulum stress, hypoxic stress, and reactive oxygen species in the sorafenib-resistant cells may facilitate development of stress pathway-specific drugs so as to enhance the efficacy of sorafenib and improve the treatment of HCC.

P27 is a protein that plays a critical role in regulating the cell cycle and cell growth (Kiyokawa et al. 1996). It functions as a cyclin-dependent kinase inhibitor by inhibiting the activity of cyclin-dependent kinases. In normal cells, p27 levels are tightly regulated, and its expression is high in cells that are not dividing. However, in cancer cells, p27 expression is often downregulated, allowing the cells to bypass normal cell cycle checkpoints and continue to grow and divide uncontrollably. Such type of negative association between p27 abundance and prognosis has been observed a various type of cancers, including colon cancer, breast cancer, prostate cancer, lung cancer, and liver cancer etc. (Lloyd et al. 1999; Slingerland and Pagano 2000). This study found that NEDD8-mediated CUL1 neddylation modification enhanced SCF ubiquitin ligase complex to link to p27 and subsequently induced K29-linked polyubiquitin chains to be added to p27. This facilitated the degradation of ubiquitinated p27 protein by enhancing autophagy flux. The autophagy-lysosome-mediated degradation probably plays more important role in p27

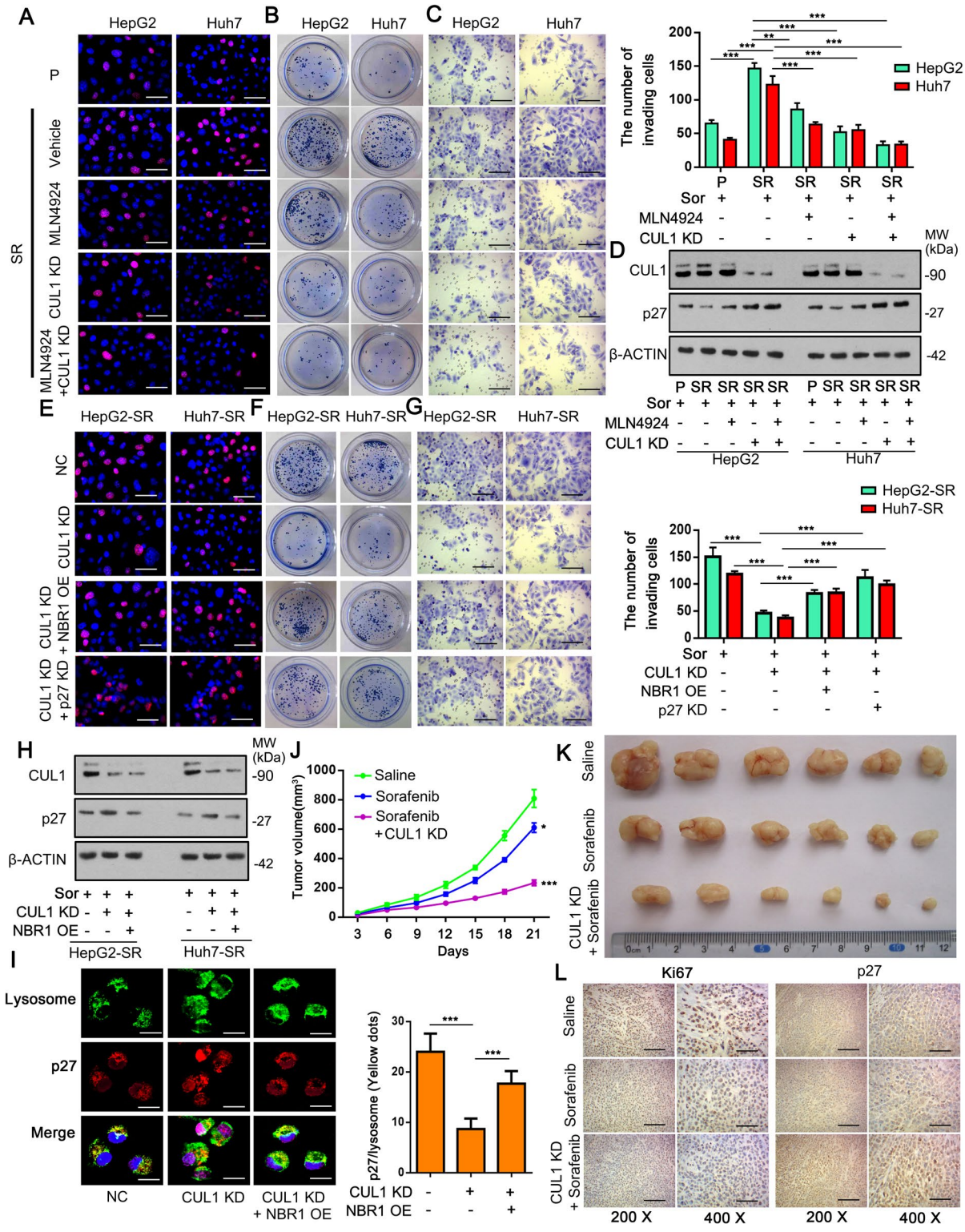
A
HepG2
Huh7
P
SR
Vehicle
MLN4924
CUL1 KD
MLN4924 +CUL1 KD
B
C
The number of invading cells
HepG2
Huh7
P SR SR SR SR
Sor + + + + +
MLN4924 - - + - +
CUL1 KD - - - + +
D
MW (kDa)
CUL1
p27
β-ACTIN
-90
-27
-42
HepG2
Huh7
E
HepG2-SR
Huh7-SR
NC
CUL1 KD
CUL1 KD + NBR1 OE
CUL1 KD + p27 KD
F
G
HepG2-SR
Huh7-SR
CUL1 KD + NBR1 OE
p27 KD
H
I
Lysosome
p27
Merge
NC
CUL1 KD
CUL1 KD + NBR1 OE
p27/lysosome (Yellow dots)
J
Saline
Sorafenib
Sorafenib +CUL1 KD
Tumor volume(mm³)
Days
K
Saline
Sorafenib
CUL1 KD + Sorafenib
L
Ki67
p27
200 X
400 X

◂**Fig. 7** Blocking neddylation and Cul1-NBR1 restores drug sensitivity in sorafenib-resistant cells (**A**) EdU incorporation assay showing reduced proliferation or activity of sorafenib-resistant cells under the conditions of CUL1 knockdown or MLN4924 treatment (1 μM). (**B**) Colony formation assay demonstrating decreased colony formation of sorafenib-resistant cells culture under the conditions of CUL1 knockdown or MLN4924 treatment (1 μM). (**C**) Transwell assay demonstrating inhibited invasion of sorafenib-resistant cells under the conditions of CUL1 knockdown or MLN4924 treatment (1 μM). (**D**) Western blot analysis demonstrating changes in p27 protein levels under conditions of CUL1 silencing with or without simultaneous addition of MLN4924 (1 μM). (**E**) EdU incorporation, (**F**) Colony formation and (**G**) Transwell assays show increased proliferation, colony formation and invasion when over-expressing NBR1 or knocking down p27 in CUL1 knockdown sorafenib-resistant cells. (**H**) Western blot showing re-stabilized p27 protein when over-expressing NBR1 in CUL1 knockdown sorafenib-resistant cells. (**I**) CUL1 knockdown reduced the immunofluorescence of p27 merged with the immunofluorescence of lysosomes. However, over-expressing NBR1 attenuated the effect by CUL1 knockdown. (**J and K**) Tumor volume and growth images demonstrating largely reduced xenografted tumor volume by day 21 after subcutaneous injection of CUL1 knocked down sorafenib-resistant HepG2 cells. (**L**) Representative immunohistochemistry images showing reduced proliferating marker Ki67 and increased p27 protein expression in CUL1 knocked down sorafenib-resistant HepG2 cell-derived xenografted tumors. $^{*}P<0.05$, $^{**}P<0.01$ and $^{***}P<0.001$ ($n=3$ in study *in vitro* and $n=6$ in study *in vivo*)

protein degradation than ubiquitin–proteasome-mediated protein degradation, because BafA1 exhibited a stronger stabilizing effect than MG132 in p27 protein. The K29-linked polyubiquitin chains on p27 probably induced the degradation of p27 in lysosome rather than in proteasome. It has been reported that K29-linked polyubiquitin chains prefer to induce protein degradation in lysosome, while K48-linked polyubiquitin chains more likely induce protein degradation in proteasome (Feng et al. 2019; Chastagner et al. 2006). Our study further confirmed that restoring p27 expression attenuates the acquired sorafenib resistance in HCC patients.

We found that mRNAs of autophagy receptors SQSTM1 and NBR1 are upregulated in the drug-resistant cells, but their protein level were reduced. The results were line with the enhanced autophagy in the drug-resistant cells. The increased NBR1 and SQSTM1 mRNA contributes to their protein levels and the formation of autophagosomes in early autophagy, but the degradation of autophagosomes in lysosomes in later autophagy leads to the final reduction of NBR1 and SQSTM1 proteins. SQSTM1, also termed p62, is the first selected autophagy adaptor identified in mammals (Bjorkoy et al. 2005). SOSTM1/p62 binds directly to Atg8/LC3 to facilitate degradation of ubiquitinated protein aggregates by autophagy (Pankiv et al. 2007). In this study, SQSTM1 knockdown greatly abrogated high basal level of autophagy in sorafenib-resistant cells by inhibiting autophagic lysosome formation. SQSTM1 is required for selective macroautophagy by acting as a a bridge between polyubiquitinated proteins and autophagosomes. They promotes the recruitment of ubiquitinated cargo proteins to autophagosomes. SQSTM1 knockdown impairs the transport of polyubiquitinated proteins to autophagosomes, thereby suppressing the degradation of the polyubiquitinated proteins with autophagosomes in lysosomes. It probably leads to the accumulation of autophagosomes in cells, which is line with the increase of autophagosomes after SQSTM1 knockdown. The formation of autophagosomes and lysosomes to autolysosomes is blocked after the SQSTM1 knockdown, which probably results in the reduction of autolysosomes. Previous studies showed that NBR1 physically binds to p62 and forms oligomers in selective autophagy of ubiquitinated targets (Kirkin et al. 2009a; Lamark et al. 2009). However, later research demonstrated that NBR1 alone is sufficient for the degradation of polyubiquitinated proteins as evidenced by autophagosomal clearance of NBR1 in p62-deficient cells (Kirkin et al. 2009b), which is consistent to our current observation that overexpression of NBR1 rescued the reduced autophagic flow as well as reduced p27 protein levels in SQSTM1 knockdown cells.

The bioinformatics analysis showed that MDM2 is not only increased in cancerous than normal tissues but also elevated in sorafenib non-responder than responder cancer. MDM2 is not only a E3 ubiquitin ligase, but also E3 NEDD8 ligase (Wolf

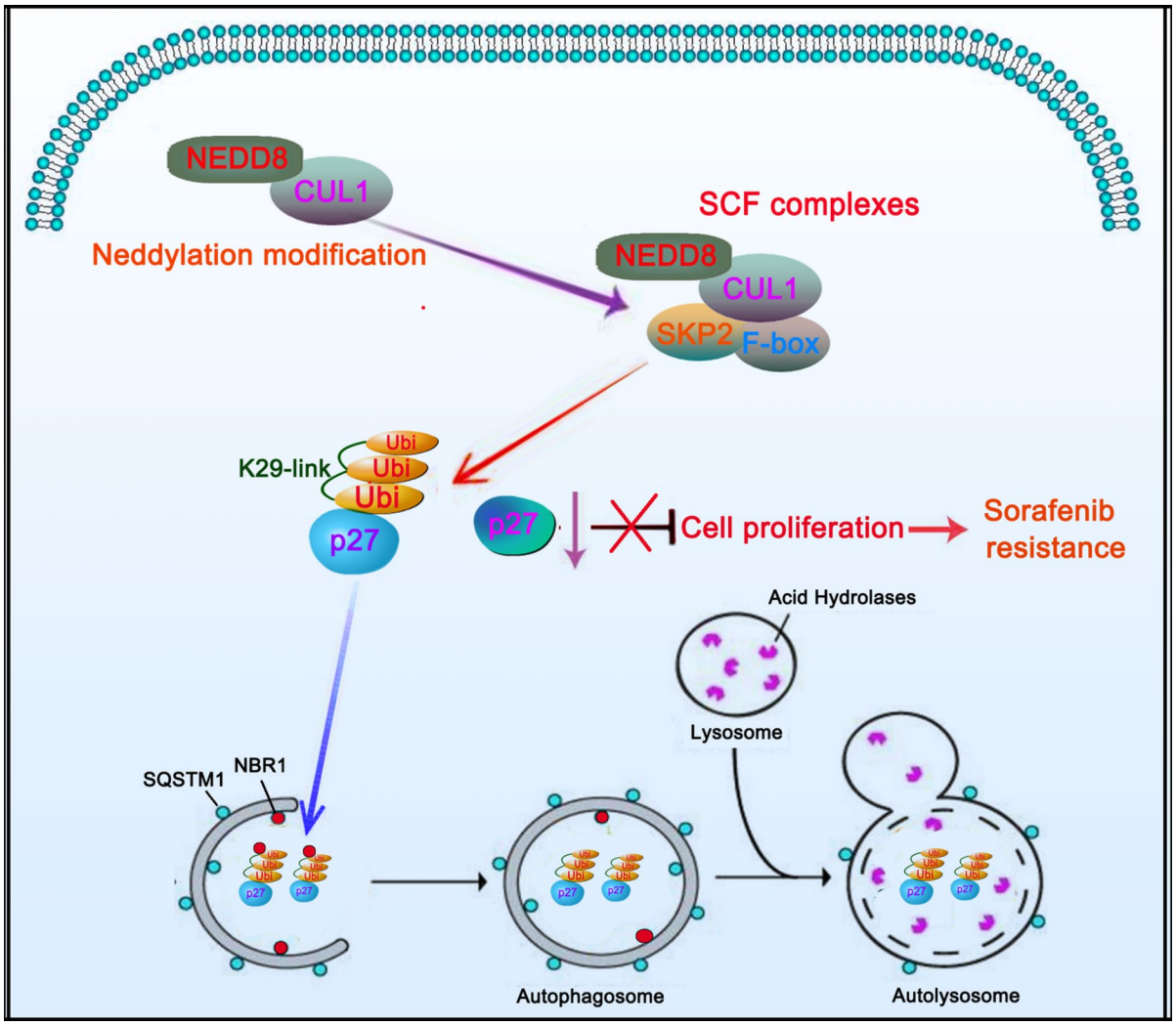

Fig. 8 The mechanism diagram that CUL1-neddylation mediated p27 degradation contributes to sorafenib resistance in liver cancer. NEDD8-mediated CUL1 neddylation modification enhances SCF ubiquitin ligase complex to target p27 and subsequently induced K29-linked polyubiquitin chains to be added to p27. Furthermore, NBR1 facilitates the degradation of ubiquitinated p27 protein by enhancing autophagy flux. Through the degradation of p27, liver cancer cells develop resistance to sorafenib

et al. 2020). Therefore, the increased MDM2 might facilitate to the neddylation modification. Indeed, as indicated by western blot assay, the knockdown of MDM2 decreased the CUL1 neddylation, but had no effect on the total protein level of CUL1 and SKP2. Further study is warranted to determine how MDM2 choices to function as an E3 NEDD8 ligase or an E3 ubiquitin ligase in sorafenib-resistant liver cancer.

In summary, we uncovered that autophagy contributed to CUL1-neddylation mediated p27 degradation in sorafenib-resistant liver cancer cells. The Mechanism diagram is shown in Fig. 8. Blocking neddylation or autophagy can restore drug sensitivity, which provides a novel strategy to achieve effective anti-tumor therapy in the future.

Acknowledgements The author sincerely thanks the GEO, TCGA, cBioPortal, and GEPIA databases, and also pays tribute to the patients who provided tumor tissues for the research.

Author contributions Conceptualization, H.T. X, S.Y.Z; methodology, H.T. X, S.Y.Z, Q.Q.Z, Y.X; software, H.B.Z, T.M.H, X.L.Z. and S.Y.Z.; formal analysis, Y.X, H.B.Z, T.M.H, X.L.Z, J.T.E; investigation, X.L.Z, J.T.E, X.D.L, R.T.W; resources, Q.Q.Z, Y.X, H.B.Z, T.M.H; data curation, X.D.L, R.T.W, H.Y.L, R.X; writing—original draft preparation, X.D.L, R.T.W, H.Y.L, R.X; writing—review and editing, X.D.L, R.T.W, H.Y.L, R.X; visualization, H.T. X, S.Y.Z, Q.Q.Z, Y.X; supervision, H.T. X, S.Y.Z, Q.Q.Z, Y.X; project administration, X.D.L, R.T.W, H.Y.L, R.X; funding acquisition, R.X..

Funding This work was supported by the National Natural Science Foundation of China (Grant No. 82073301), Climing program of Harbin Medical University Cancer Hospital (Grant No. PDYS2024-16), Haiyan Research Fund of Harbin Medical University Cancer Hospital (Grant No. JJZD2024-29).

Data availability Data is provided within the manuscript or supplementary information files. Other materials and data supporting the research results can be reasonably obtained from the corresponding author.

Declarations

Informed consent statement Informed consent was obtained from all subjects involved in the study.

Institutional review board statement This study was approved by the Ethics Committee of the Harbin Medical University Cancer Hospital (Approved number: KY2023-32. Date:2023.3.10). Written informed consent was obtained from all participants.

Conflicts of interest The authors declare no competing interests.

References

Bjorkoy G, Lamark T, Brech A, Outzen H, Perander M, Overvatn A, Stenmark H, Johansen T. p62/SQSTM1 forms protein aggregates degraded by autophagy and has a protective effect on huntingtin-induced cell death. J Cell Biol. 2005;171:603–14.

Cainap C, Qin S, Huang WT, Chung IJ, Pan H, Cheng Y, Kudo M, Kang YK, Chen PJ, Toh HC, Gorbunova V, Eskens FA, Qian J, McKee MD, Ricker JL, Carlson DM, El-Nowiem S. Linifanib versus Sorafenib in patients with advanced hepatocellular carcinoma: results of a randomized phase III trial. J Clin Oncol. 2015;33:172–9.

Chastagner P, Israël A, Brou C. Itch/AIP4 mediates Deltex degradation through the formation of K29-linked polyubiquitin chains. EMBO Rep. 2006;7(11):1147–53.

Chen RH, Chen YH, Huang TY. Ubiquitin-mediated regulation of autophagy. J Biomed Sci. 2019a;26:80.

Chen W, Yang J, Zhang Y, Cai H, Chen X, Sun D. Regorafenib reverses HGF-induced sorafenib resistance by inhibiting epithelial-mesenchymal transition in hepatocellular carcinoma. FEBS Open Bio. 2019b;9:335–47.

Cheng AL, Kang YK, Lin DY, Park JW, Kudo M, Qin S, Chung HC, Song X, Xu J, Poggi G, Omata M, Pitman Lowenthal S, Lanzalone S, Yang L, Lechuga MJ, Raymond E. Sunitinib versus sorafenib in advanced hepatocellular cancer: results of a randomized phase III trial. J Clin Oncol. 2013;31:4067–75.

Ciechanover A, Schwartz AL. The ubiquitin-proteasome pathway: the complexity and myriad functions of proteins death. Proc Natl Acad Sci U S A. 1998;95:2727–30.

Das G, Shravage BV, Baehrecke EH. Regulation and function of autophagy during cell survival and cell death. Cold Spring Harb Perspect Biol. 2012;4:a008813.

Enchev RI, Schulman BA, Peter M. Protein neddylation: beyond cullin-RING ligases. Nat Rev Mol Cell Biol. 2015;16:30–44.

Feng X, Jia Y, Zhang Y, Ma F, Zhu Y, Hong X, Zhou Q, He R, Zhang H, Jin J, Piao D, Huang H, Li Q, Qiu X, Zhang Z. Ubiquitination of UVRAG by SMURF1 promotes autophagosome maturation and inhibits hepatocellular carcinoma growth. Autophagy. 2019;15(7):1130–49.

Hua F, Li K, Yu JJ, Lv XX, Yan J, Zhang XW, Sun W, Lin H, Shang S, Wang F, Cui B, Mu R, Huang B, Jiang JD, Hu ZW. TRB3 links insulin/IGF to tumour promotion by interacting with p62 and impeding autophagic/proteasomal degradations. Nat Commun. 2015;6:7951.

Huang J, Pan W, Ou D, Dai W, Lin Y, Chen Y, Chen X. LC3B, a protein that serves as an autophagic marker, modulates Angiotensin II-induced myocardial hypertrophy. J Cardiovasc Pharmacol. 2015;66:576–83.

Johnson PJ, Qin S, Park JW, Poon RT, Raoul JL, Philip PA, Hsu CH, Hu TH, Heo J, Xu J, Lu L, Chao Y, Boucher E, Han KH, Paik SW, Robles-Avina J, Kudo M, Yan L, Sobhonslidsuk A, Komov D, Decaens T, Tak WY, Jeng LB, Liu D, Ezzeddine R, Walters I, Cheng AL. Brivanib versus sorafenib as first-line therapy in patients with unresectable, advanced hepatocellular carcinoma: results from the randomized phase III BRISK-FL study. J Clin Oncol. 2013;31:3517–24.

Kirkin V, Lamark T, Johansen T, Dikic I. NBR1 cooperates with p62 in selective autophagy of ubiquitinated targets. Autophagy. 2009a;5:732–3.

Kirkin V, Lamark T, Sou YS, Bjorkoy G, Nunn JL, Bruun JA, Shvets E, McEwan DG, Clausen TH, Wild P, Bilusic I, Theurillat JP, Overvatn A, Ishii T, Elazar Z, Komatsu M, Dikic I, Johansen T. A role for NBR1 in autophagosomal degradation of ubiquitinated substrates. Mol Cell. 2009b;33:505–16.

Kiyokawa H, Kineman RD, Manova-Todorova KO, Soares VC, Hoffman ES, Ono M, Khanam D, Hayday AC, Frohman LA, Koff A. Enhanced growth of mice lacking the cyclin-dependent kinase inhibitor function of p27(Kip1). Cell. 1996;85:721–32.

Kocaturk NM, Gozuacik D. Crosstalk between mammalian autophagy and the ubiquitin-proteasome system. Front Cell Dev Biol. 2018;6:128.

Kudo M, Finn RS, Qin S, Han KH, Ikeda K, Piscaglia F, Baron A, Park JW, Han G, Jassem J, Blanc JF, Vogel A, Komov D, Evans TRJ, Lopez C, Dutcus C, Guo M, Saito K, Kraljevic S, Tamai T, Ren M, Cheng AL. Lenvatinib versus sorafenib in first-line treatment of patients with unresectable hepatocellular carcinoma: a randomised phase 3 non-inferiority trial. Lancet. 2018;391:1163–73.

Lamark T, Kirkin V, Dikic I, Johansen T. NBR1 and p62 as cargo receptors for selective autophagy of ubiquitinated targets. Cell Cycle. 2009;8:1986–90.

Lanczky A, Gyorffy B. Web-Based Survival Analysis Tool Tailored for Medical Research (KMplot): Development and Implementation. J Med Internet Res. 2021;23:e27633.

Lee DH, Goldberg AL. Proteasome inhibitors: valuable new tools for cell biologists. Trends Cell Biol. 1998;8:397–403.

Lin X, Han L, Weng J, Wang K, Chen T. Rapamycin inhibits proliferation and induces autophagy in human neuroblastoma cells. Biosci Rep. 2018;38:BSR20181822.

Liu J, Fan L, Wang H, Sun G. Autophagy, a double-edged sword in anti-angiogenesis therapy. Med Oncol. 2016;33:10.

Livak KJ, Schmittgen TD. Analysis of relative gene expression data using real-time quantitative PCR and the 2(-Delta Delta C(T)) Method. Methods. 2001;25:402–8.

Lloyd RV, Erickson LA, Jin L, Kulig E, Qian X, Cheville JC, Scheithauer BW. p27kip1: a multifunctional cyclin-dependent kinase inhibitor with prognostic significance in human cancers. Am J Pathol. 1999;154:313–23.

Luo Z, Yu G, Lee HW, Li L, Wang L, Yang D, Pan Y, Ding C, Qian J, Wu L, Chu Y, Yi J, Wang X, Sun Y, Jeong LS, Liu J, Jia L. The Nedd8-activating enzyme inhibitor MLN4924 induces autophagy and apoptosis to suppress liver cancer cell growth. Cancer Res. 2012;72:3360–71.

Mauvezin C, Neufeld TP. Bafilomycin A1 disrupts autophagic flux by inhibiting both V-ATPase-dependent acidification and Ca-P60A/SERCA-dependent autophagosome-lysosome fusion. Autophagy. 2015;11:1437–8.

McGlynn KA, Petrick JL, El-Serag HB. Epidemiology of Hepatocellular Carcinoma. Hepatology. 2021;73(Suppl 1):4–13.

Pankiv S, Clausen TH, Lamark T, Brech A, Bruun JA, Outzen H, Overvatn A, Bjorkoy G, Johansen T. p62/SQSTM1 binds directly to Atg8/LC3 to facilitate degradation of ubiquitinated protein aggregates by autophagy. J Biol Chem. 2007;282:24131–45.

Parazzi PL, Marson FA, Ribeiro MA, de Almeida CC, Martins LC, Paschoal IA, Toro AA, Schivinski CI, Ribeiro JD. Ventilatory abnormalities in patients with cystic fibrosis undergoing the submaximal treadmill exercise test. BMC Pulm Med. 2015;15:63.

Pinyol R, Montal R, Bassaganyas L, Sia D, Takayama T, Chau GY, Mazzaferro V, Roayaie S, Lee HC, Kokudo N, Zhang Z, Torrecilla S, Moeini A, Rodriguez-Carunchio L, Gane E, Verslype C, Croitoru AE, Cillo U, de la Mata M, Lupo L, Strasser S, Park JW, Camps J, Sole M, Thung SN, Villanueva A, Pena C, Meinhardt G, Bruix J, Llovet JM. Molecular predictors of prevention of recurrence in HCC with sorafenib as adjuvant treatment and prognostic factors in the phase 3 STORM trial. Gut. 2019;68:1065–75.

Sapi J, Kovacs L, Drexler DA, Kocsis P, Gajari D, Sapi Z. Tumor volume estimation and quasi-continuous administration for most effective bevacizumab therapy. PLoS ONE. 2015;10:e0142190.

Sarveazad A, Agah S, Babahajian A, Amini N, Bahardoust M. Predictors of 5 year survival rate in hepatocellular carcinoma patients. J Res Med Sci. 2019;24:86.

Shintani T, Klionsky DJ. Autophagy in health and disease: a double-edged sword. Science. 2004;306:990–5.

Siegel RL, Miller KD, Wagle NS, Jemal A. Cancer statistics, 2023. CA Cancer J Clin. 2023;73:17–48.

Slingerland J, Pagano M. Regulation of the cdk inhibitor p27 and its deregulation in cancer. J Cell Physiol. 2000;183:10–7.

Tang Z, Li C, Kang B, Gao G, Li C, Zhang Z. GEPIA: a web server for cancer and normal gene expression profiling and interactive analyses. Nucleic Acids Res. 2017;45:W98–102.

Tang W, Chen Z, Zhang W, Cheng Y, Zhang B, Wu F, Wang Q, Wang S, Rong D, Reiter FP, De Toni EN, Wang X. The mechanisms of sorafenib resistance in hepatocellular carcinoma: theoretical basis and therapeutic aspects. Signal Transduct Target Ther. 2020;5:87.

Wei J, Wang Z, Wang W, Liu X, Wan J, Yuan Y, Li X, Ma L, Liu X. Oxidative stress activated by sorafenib alters the temozolomide sensitivity of human glioma cells through autophagy and JAK2/STAT3-AIF axis. Front Cell Dev Biol. 2021;9:660005.

White E, DiPaola RS. The double-edged sword of autophagy modulation in cancer. Clin Cancer Res. 2009;15:5308–16.

Wilhelm SM, Adnane L, Newell P, Villanueva A, Llovet JM, Lynch M. Preclinical overview of sorafenib, a multikinase inhibitor that targets both Raf and VEGF and PDGF receptor tyrosine kinase signaling. Mol Cancer Ther. 2008;7:3129–40.

Willatt JM, Francis IR, Novelli PM, Vellody R, Pandya A, Krishnamurthy VN. Interventional therapies for hepatocellular carcinoma. Cancer Imaging. 2012;12:79–88.

Wolf ER, Mabry AR, Damania B, Mayo LD. Mdm2-mediated neddylation of pVHL blocks the induction of antiangiogenic factors. Oncogene. 2020;39(29):5228–39.

Wu SD, Ma YS, Fang Y, Liu LL, Fu D, Shen XZ. Role of the microenvironment in hepatocellular carcinoma development and progression. Cancer Treat Rev. 2012;38:218–25.

Yang Q, Zhao J, Chen D, Wang Y. E3 ubiquitin ligases: styles, structures and functions. Mol Biomed. 2021;2:23.

Zhai B, Hu F, Jiang X, Xu J, Zhao D, Liu B, Pan S, Dong X, Tan G, Wei Z, Qiao H, Jiang H, Sun X. Inhibition of Akt reverses the acquired resistance to sorafenib by switching protective autophagy to autophagic cell death in hepatocellular carcinoma. Mol Cancer Ther. 2014;13:1589–98.

Zheng YC, Guo YJ, Wang B, Wang C, Mamun MAA, Gao Y, Liu HM. Targeting neddylation E2s: a novel therapeutic strategy in cancer. J Hematol Oncol. 2021;14:57.